Heteroleptic binuclear palladium(II) and platinum(II) complexes containing 1,2-bis(diphenylphosphino)acetylene and 1,2-benzenedithiolates: syntheses, crystal structures, electrochemistry and photoluminescence properties†

Kyong-Soon Shin,[a] Kyung-In Son,[a] Jae Il Kim,[b] Chang Seop Hong,[b] Myungkoo Suh‡[c] and Dong-Youn Noh*[a]

Received 28th August 2008, Accepted 28th November 2008
First published as an Advance Article on the web 28th January 2009
DOI: 10.1039/b815013c

A series of heteroleptic binuclear Pd(II) and Pt(II) complexes, $[M(bdts)]_2(\mu\text{-dppa})_2$ (M = Pd (**3**) and Pt (**4**); dppa = 1,2-bis(diphenylphosphino)acetylene = $Ph_2PC{\equiv}CPPh_2$; bdts = 1,2-benzenedithiolate (bdt: **a**), 3,4-toluenedithiolate (tdt: **b**) and 1,4-dichloro-2,3-benzenedithiolate (Cl_2bdt: **c**), containing two square-planar MP_2S_2 cores were prepared using $(MCl_2)_2(\mu\text{-dppa})_2$ (M = Pd (**1**) and Pt (**2**)) and the corresponding 1,2-benzenedithiols, and characterized by spectroscopic methods including FT-IR, Raman, UV-vis, MALDI-TOF-MS, $^{31}P\{^1H\}$ and/or $^{195}Pt\{^1H\}$ NMR spectroscopy. X-Ray crystal structure analyses for complexes **3** and **4** revealed that C1C2C4C3 is twisted in two ways with a torsion angle of 21.6–30.7° for **3a**, **3b**, **4a** and **4b** and about 42° for **3c** and **4c**, and that their crystals are racemic mixtures. Due to the more electronegative chloride atoms in the ligand, complexes **3c** and **4c** show higher ν(M–S) vibrational frequencies in their Raman spectra, smaller spin–spin coupling constants (J_{Pt-P}) in their $^{195}Pt\{^{31}P\}$ NMR spectra and higher anodic potentials (E_{pa}) in their cyclic voltammograms than complexes **3a**, **3b**, **4a** and **4b**. Moreover, only complex **4c** containing the chlorinated ligand and Pt(II) ion exhibits luminescence (λ_{ob} = 610 nm and λ_{ex} = 440 nm) in the solid state at 298 K. This emissive transition can be assigned as the $d\text{–}\pi^*_{dithiolate}$ metal-to-ligand charge transfer (MLCT) and the feasibility of this spin-forbidden transition is ascribed to the effective spin–orbit coupling of ligand **c** containing heavy chloride atoms and the large spin–orbit coupling in Pt(II).

Introduction

A considerable amount of interests has been devoted to the chemistry of palladium(II) and platinum(II) complexes, mostly focusing on their structural diversity, anticancer activity, catalytic effect and photochemical properties, as well as their superconductivity.[1–35] These properties are basically related to the characteristic coordination preference of Pd(II) and Pt(II) ions for square-planar geometry. These complexes are mostly mononuclear system with C_2MP_2,[3] S_2MN_2,[4,5] MP_4[6] and S_2MP_2[7–13] cores where M = Pd(II) or Pt(II), and the ligands are monodentate or chelate systems. One of the relevant diphosphine chelate ligands is 1,1′-bis(diphenylphosphino)ferrocene (dppf) (Scheme 1), which is frequently comprised of $(dppf)MS_2$ complexes where S_2 is dithiolate ligand such as 1,2-benzenedithiolates,[14] 1,2-ethylenedithiolates,[15] or tetrathiafulvalene-2,3-dithiolates.[16] These complexes show considerable interactive redox behaviors among the redox-active centers such as dppf, M(II) ions and dithiolate ligands. Linear diphosphine ligands such as *trans*-1,2-bis(diphenylphosphino)ethane (*trans*-dppen),[17] 1,4-bis(diphenylphosphino)butadiyne (dppby),[18] 1,4-bis(diphenylphosphino)-benzene (dppb)[19] and 4,4′-bis(diphenylphosphino)biphenylene (dpbp)[20] are also used as bridging ligands between two metal ions, mostly resulting in a binuclear complex as the main product. The dppby ligand also adopts a trinuclear system as a minor product.[18] It is interesting to note that the complexes with *trans*-dppen and dppby ligands undergo intramolecular cyclization when subjected to UV-irradiation or elevated temperatures.

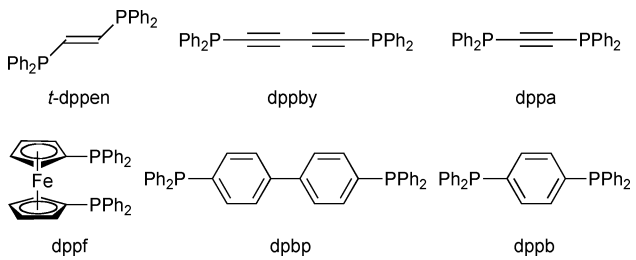

Scheme 1

Another linear diphosphine ligand that we are interested in is 1,2-bis(diphenylphosphino)acetylene (dppa: $Ph_2PC{\equiv}CPPh_2$). It was utilized for the first time by Carty, as a bridging ligand between two metal ions.[21,22] Following these reports, many binuclear complexes, together with mono- and multi-nuclear complexes,

[a]*Department of Chemistry, Seoul Women's University, Seoul, 139-774, Korea. E-mail: dynoh@swu.ac.kr; Fax: +82 2 970 5972; Tel: +82 2 970 5656*
[b]*Department of Chemistry, Korea University, Seoul, 136-701, Korea. E-mail: cshong@korea.ac.kr; Fax: +82 2 3290 3121; Tel: +82 2 3290 3138*
[c]*Department of Chemistry, Sungkyunkwan University, Suwon, 440-746, Korea. E-mail: msuh@skku.edu; Fax: +82 31 290 7075; Tel: +82 31 290 5941*

† Electronic supplementary information (ESI) available: Cyclic voltammograms of **2**, **3** and **4**, the crystal packing diagrams of **3** and **4**, and UV-Vis, ^{31}P NMR and ^{195}Pt NMR spectra of **1**, **2**, **3** and **4**. CCDC reference numbers 699934–699939. For ESI and crystallographic data in CIF or other electronic format see DOI: 10.1039/b815013c

‡ Present address: Department of Chemistry and Advanced Materials Science, Kyung Hee University, Yongin 446-701, Korea.

of Ni(0), Cr(0), Mo(0), W(0), Os(0), Cu(I), Ag(I), Au(I), Mn(I), Ru(II), Hg(II) and mixed Pd(II)/Pt(II) ions have been reported, which comprise 1 ~ 4 dppa bridging ligands and diverse terminal ligands such as halides (Cl, Br, I, SCN), CO, cyclopentadienyl, alkyl, acetylacetonato (acac), phosphine, monothiol and so on.[21–33] All of these reports, however, deal solely with the synthesis, X-ray crystal structure analysis and electrochemical properties (only in some reports) of the complexes, whereas the specific properties of the complexes, such as their luminescence, have not been reported.

Very recently, we investigated and reported the X-ray structure analysis and luminescence properties of binuclear Pt(II)-dppa complexes with the bidentate 1,2-ethylenedithiolate ligands, ([Pt(1,2-dithiolate)]$_2$(μ-dppa)$_2$).[34,35] To the best of our knowledge, this is the first, albeit preliminary, report concerning the luminescence properties of binuclear metal–dppa complexes. Furthermore, the luminescence properties of Pt-complexes with a P_2PtS_2 core have not been investigated as much as those with an N_2PtS_2[4,5] or C_2PtS_2[3] core. In this paper, we describe the results of our systematic investigation of the [M(1,2-dithiolate)]$_2$(μ-dppa)$_2$ complexes where M = Pd(II) or Pt(II), and the 1,2-dithiolate ligand is 1,2-benzenedithiolate (**a**), 3,4-toluenedithiolate (**b**) or 1,4-dichloro-2,3-benzenedithiolate (**c**). The luminescence properties of the complexes are explained in correlation with the FT-IR, Raman and ^{195}Pt{^{31}P} NMR spectra, cyclic voltammetry results and X-ray crystal structure analysis, and are compared with those of other luminescent complexes with a P_2PtS_2 core.

Experimental

The reagent-grade chemicals used for the syntheses were commercially purchased and used without further purification. For example, commercially obtained 3,6-dichloro-1,2-benzendithiol (H_2**c**) containing an inseparable 5% 1,2-benzenedithiol impurity was used without further purification. The solvents were degassed by Ar-bubbling prior to use. All reactions and recrystallizations involving the Pd(II) and Pt(II) complexes were performed under protection from light and air.

The measurements of the MALDI-TOF-MS and elemental analyses were carried out at the National Center for Inter-University Research Facilities (NCIRF) in Seoul. The Raman spectra were recorded with a Raman microscope spectrometer (Renishaw, Ltd.) equipped with a He–Ne laser (λ_o = 6328 Å). A low laser power of *ca.* 0.06 mW focused on a 1 μm^2 area was used. The infrared spectra were recorded by the KBr method on a MIDAC FT-IR spectrophotometer in the range of 4000–400 cm^{-1}. The ^{1}H NMR spectra were recorded using an Avance 500 (Bruker) spectrometer with the samples dissolved in $CDCl_3$. The ^{31}P{^{1}H} and ^{195}Pt{^{1}H} NMR spectra of the complexes dissolved in $CDCl_3$ or CD_2Cl_2 were recorded using an Avance 500 (Bruker) or DMX 600 (Bruker) spectrometer at 202.46 MHz and 128.38 MHz, respectively. The positive chemical shifts are downfield from external standards, *viz* 85% H_3PO_4 for the ^{31}P{^{1}H} resonances and 1.0 M K_2PtCl_4 in D_2O for the ^{195}Pt{^{1}H} resonances. The ^{31}P{^{1}H} and ^{195}Pt{^{1}H} NMR data and coupling parameters for complexes **1**, **2**, **3** and **4** are summarized in Tables 1 and 2. The cyclic voltammetry (CV) measurements were performed at room temperature with a CHI 620A Electrochemical Analyzer (CHI Instrument Inc.) in 10 mL CH_2Cl_2 solution containing a 1.0 mM sample, using 0.1 M n-Bu_4NBF_4 as a supporting electrolyte, Ag/Ag$^+$ as the reference electrode, a Pt-button working electrode (r = 1 mm), a Pt-wire as the counter electrode and with a scan rate of 50 mV s^{-1}. All redox potentials were referenced against the Fc/Fc$^+$ couple ($E_{1/2}$ = +0.687 V). The UV-Vis spectra were obtained at ambient temperature in acetonitrile on an HP 8452A diode array spectrophotometer. The emission spectra of the microcrystalline samples were acquired at ambient temperature using an Amico-Bowman Series 2 spectrofluorometer equipped with a 7 W pulsed Xe Lamp. The Pt(II) samples were excited with 440 nm light and the luminescence was collected for 5 ms after a 10 μs delay in order to reduce the scattering excitation light. The excitation spectra were observed with the parameters λ_{obs} = 610 nm, a 16/16 band pass filter and 700 V. The emission spectra were observed with the parameters λ_{ex} = 440 nm, a 16/16 band pass filter and 680 V.

Table 1 ^{31}P{^{1}H} NMR data for the complexes **1** and **3**[a]

	δ_H[b]/ppm	δ_P[c]/ppm	$^nJ_{H-H}$/Hz
1	7.53468 (16H, q; H1)	4.873	
	7.48212 (8H, t; H3)		^3J = 7.47
	7.25642 (16H, t; H2)		
3a	7.48693 (16H, q; H1)	1.757	
	7.42107 (8H, t; H3)		^3J = 7.40
	7.21785 (16H, t; H2)		^3J = 7.40
	7.14599 (4H, dd; H4 + H7)		^3J = 5.95, ^4J = 3.22
	6.82061 (4H, dd; H5 + H6)		^3J = 5.95, ^4J = 3.22
3b	7.48316 (16H, m; H1)	1.676	
	7.41270 (8H, t; H3)		^3J = 7.40
	7.20997 (16H, t; H2)		^3J = 7.40
	7.01595 (2H, d; H4)		^3J = 8.00
	6.96357 (2H, s; H7)		
	6.63725 (2H, d; H5)		^3J = 8.00
	2.16880 (6H, s; H6)		
3c	7.49647 (16H, q; H1)	1.943	
	7.44636 (8H, t; H3)		^3J = 7.40
	7.24612 (16H, t; H2)		^3J = 7.40
	6.91114 (4H, s; H5 + H6)		

[a] 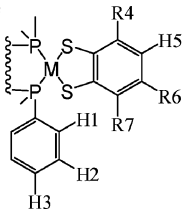

(**3a**) and (**4a**): R4 = R6 = R7 = H
(**3b**) and (**4b**): R4 = R7 = H; R6 = CH_3
(**3c**) and (**4c**): R4 = R7 = Cl; R6 = H

[b] d: doublet; t: triplet; q: quartet; dd: doublet of doublets; m: multiplet. [c] Positive chemical shifts are downfield from the standard (85% H_3PO_4).

X-Ray crystal structure determinations

Single crystals of complexes **3** and **4** suitable for the X-ray structure analysis were obtained by the recrystallization of the purified complexes from $CHCl_3$–MeOH or CH_2Cl_2–MeOH. The X-ray crystallographic data for these complexes were collected on a Bruker SMART APEXII diffractometer equipped with graphite-monochromated Mo-Kα radiation (λ = 0.71073 Å). The preliminary orientation matrix and cell parameters were determined from three sets of ω/ψ or ω scans at different starting angles. The data frames were obtained at scan intervals of 0.5° with an exposure time of 10 s per frame for complexes **3a**, **3b**, **4a** and **4b**, and 20 s per frame for complexes **3c** and **4c**. The reflection data were corrected for Lorentz and polarization factors.

Table 2 $^{195}Pt\{^{1}H\}$ and $^{31}P\{^{1}H\}$ NMR data for the complexes **2** and **4**[a]

	δ_H[b]/ppm	δ_P[c]/ppm	δ_{Pt}[c]/ppm	$^nJ_{H-H}$/Hz	$^1J_{Pt-P}$/Hz
2	7.55808 (16H, q; H1)	–13.753	–4431		3660
	7.47198 (8H, t; H3)			$^3J = 7.35$	
	7.24063 (16H, t; H2)			$^3J = 7.35$	
4a	7.49668 (16H, q; H1)	–4.504	–4729		2814
	7.39078 (8H, t; H3)			$^3J = 7.33$	
	7.33699 (4H, dd; H4 + H7)			$^3J = 5.85$, $^4J = 3.22$	
	7.21153 (16H, t; H2)			$^3J = 7.33$	
	6.76139 (4H, dd; H5 + H6)			$^3J = 5.85$, $^4J = 3.22$	
4b	7.49291 (16H, m; H1)	–4.502	–4726		2813
	7.39078 (8H, t; H3)			$^3J = 7.33$	
	7.20348 (18H, t; H2 + H4)				
	7.14535 (2H, s; H7)				
	6.58692 (2H, d; H5)			$^3J = 8.11$	
	2.18978 (6H, s; H6)				
4c	7.50837 (16H, q; H1)	–4.947	–4700		2800
	7.42373 (8H, t; H3)			$^3J = 7.33$	
	7.24070 (16H, q; H2)				
	6.88700 (4H, s; H5 + H6)				

[a] Proton numbering scheme is found in Table 1. [b] d: doublet; t: triplet; q: quartet; dd: doublet of doublets; m: multiplet. [c] Positive chemical shifts are downfield from the standards (85% H_3PO_4 and 1.0 M K_2PtCl_4 solutions for the ^{31}P and ^{195}Pt resonances, respectively).

Absorption corrections were carried out using SADABS.[36] The structures were solved by direct methods and refined by full-matrix least-squares analysis using anisotropic thermal parameters for the non-hydrogen atoms with the SHELXTL program.[37] The chloroform molecules in complex **3a** were restrained by means of the SAME instruction. Two methylene chloride molecules for complex **3b** and two water molecules for complex **3c** were significantly disordered and could not be modeled properly, thus the program SQUEEZE,[38] a part of the PLATON package[39] of crystallographic software, was used to calculate the solvent disorder area and remove its contribution to the overall intensity data. Hydrogen atoms of the water molecules in complexes **4a**, **4b** and **4c** were not found in the difference map and then not included. One of three water molecules in complex **4a** was disordered and assigned with an occupancy factor of 0.5. The carbon atoms (C8 and C63) for complex **4b** was disordered and assigned with an occupancy factor of 0.4 : 0.6. The rigid group fittings and refinements (AFIX 66) were performed on the two disordered phenyl rings (from C47 to C58) for complex **4c**, which were placed with 0.58 : 0.42 and 0.51 : 0.49 occupancy factors, respectively. The crystallographic data and the details of the data collection are listed in Table 3, and the selected bond distances and angles are summarized in Table 4.

Preparation of the Pd(II) and Pt(II) complexes

$(PdCl_2)_2(\mu\text{-dppa})_2$ (1). An ethanol solution (75 mL) of Na_2PdCl_4 (2.4 mmol, 0.71 g) was slowly added to an ethanol solution (75 mL) of dppa (2.4 mmol, 0.95 g) with stirring at room temperature for 1 h. The yellow product was filtered off, washed

Table 3 Crystallographic data for **3a**·3$CHCl_3$, **3b**, **3c**, **4a**·3H_2O·$CHCl_3$, **4b**·2H_2O·$CHCl_3$ and **4c**·H_2O

	3a·3$CHCl_3$	**3b**	**3c**	**4a**·3H_2O·$CHCl_3$	**4b**·2H_2O·$CHCl_3$	**4c**·H_2O
Formula	$C_{67}H_{51}Cl_9P_4Pd_2S_4$	$C_{66}H_{52}P_4Pd_2S_4$	$C_{64}H_{44}Cl_4P_4Pd_2S_4$	$C_{65}H_{55}Cl_3O_3P_4Pt_2S_4$	$C_{67}H_{57}Cl_3O_2P_4Pt_2S_4$	$C_{64}H_{46}Cl_4OP_4Pt_2S_4$
M_f	1640.05	1310.00	1419.71	1632.74	1642.78	1615.11
T/K	293(2)	293(2)	293(2)	293(2)	293(2)	293(2)
Crystal system	Monoclinic	Triclinic	Monoclinic	Triclinic	Triclinic	Monoclinic
Space group	$P2_1/n$	$P\bar{1}$	$C2/c$	$P\bar{1}$	$P\bar{1}$	$C2/c$
a/Å	13.7964(3)	10.8273(7)	26.9243(13)	10.6227(12)	10.8814(8)	42.3763(16)
b/Å	14.0504(3)	14.6236(10)	17.0332(13)	14.2985(12)	14.7267(12)	11.0230(4)
c/Å	36.1985(8)	21.0611(13)	17.4498(13)	23.709(3)	21.2919(16)	31.0144(12)
α/°	90.00(0)	97.031(2)	90.00(0)	74.885(1)	97.397(2)	90.00(0)
β/°	93.538(1)	97.023(2)	124.389(5)	86.509(1)	96.961(2)	118.554(2)
γ/°	90.00(0)	91.372(2)	90.00(0)	71.508(1)	92.179(3)	90.00(0)
V/Å^3	7003.6(3)	3282.2(4)	6603.9(8)	3296.2(6)	3353.6(4)	12725.1(8)
Z	4	2	4	2	2	8
Crystal size/mm	0.36 × 0.12 × 0.15	0.1 × 0.08 × 0.07	0.20 × 0.12 × 0.03	0.19 × 0.18 × 0.17	0.1 × 0.07 × 0.07	0.12 × 0.08 × 0.06
Refl. collected	69043	54698	32067	32798	55310	59345
Refl. unique	17498	16198	8196	13065	16442	15807
R_{int}	0.0633	0.0692	0.0380	0.0290	0.0423	0.0665
R^a	0.0525	0.0472	0.0447	0.0393	0.0418	0.0517

[a] $R = \sum\|F_o\| - |F_c\|/\sum|F_o|$.

Table 4 Selected bond distances (Å), bond angles (°) and torsion angles (°) for complexes **3** and **4**[a]

	3a	3b	3c	4a	4b	4c
M(1)–P(1)	2.301(1)	2.278(1)	2.312(1)	2.258(2)	2.260(2)	2.284(2)
M(1)–P(2)	2.291(1)	2.294(1)	2.289(1)	2.278(2)	2.280(2)	2.273(2)
M(2)–P(3)	2.297(1)	2.282(1)		2.260(2)	2.258(2)	2.293(2)
M(2)–P(4)	2.283(1)	2.308(1)		2.282(2)	2.279(2)	2.275(2)
M(1)–S(1)	2.282(1)	2.293(1)	2.291(1)	2.313(2)	2.306(2)	2.300(2)
M(1)–S(2)	2.280(1)	2.289(1)	2.286(1)	2.303(2)	2.295(2)	2.297(2)
M(2)–S(3)	2.287(2)	2.291(1)		2.303(2)	2.307(2)	2.314(2)
M(2)–S(4)	2.279(1)	2.277(1)		2.301(2)	2.302(2)	2.293(2)
C(1)–C(2)	1.194(6)	1.186(5)	1.206(6)[b]	1.198(9)	1.187(8)	1.191(9)
C(3)–C(4)	1.190(6)	1.195(4)	1.183(6)[b]	1.200(9)	1.201(8)	1.177(9)
P(1)–M(1)–P(2)	95.12(4)	95.16(3)	96.78(3)	94.18(6)	95.39(5)	97.34(7)
P(1)–M(1)–S(2)	173.34(5)	172.76(3)	175.45(3)	172.66(6)	170.22(7)	172.79(7)
P(2)–M(1)–S(2)	87.46(4)	89.97(3)	87.76(3)	90.72(6)	89.72(7)	88.19(7)
P(1)–M(1)–S(1)	88.48(4)	86.02(4)	86.84(3)	86.42(6)	86.52(7)	86.19(7)
P(2)–M(1)–S(1)	176.29(5)	177.64(3)	171.76(3)	174.58(6)	177.86(7)	172.86(7)
S(2)–M(1)–S(1)	89.07(5)	88.68(4)	88.70(4)	88.19(6)	88.25(8)	88.83(7)
P(3)–M(2)–P(4)	94.23(4)	96.34(3)		95.00(6)	94.68(5)	95.75(7)
P(3)–M(2)–S(4)	171.48(5)	169.01(4)		172.25(7)	173.27(6)	174.48(8)
P(4)–M(2)–S(4)	89.45(5)	89.29(4)		89.86(7)	90.27(6)	86.98(8)
P(3)–M(2)–S(3)	87.57(5)	85.82(4)		86.50(7)	86.34(6)	89.13(7)
P(4)–M(2)–S(3)	177.28(5)	177.81(4)		177.24(7)	176.97(6)	175.12(7)
S(4)–M(2)–S(3)	89.05(5)	88.53(5)		88.41(8)	88.49(6)	88.16(8)
C(1)–C(2)–C(4)–C(3)	–30.67	27.51	–41.51[c]	21.65	–24.61	–42.13

[a] M = Pd for **3a**, **3b** and **3c**, and M = Pt for **4a**, **4b** and **4c**. [b] Bond distances corresponding to C(1)–C(1)$^{\#}$ and C(2)–C(2)$^{\#}$, respectively ($^{\#}$: $-x + 1$, y, $-z + 3/2$). [c] Torsion angle for C(1)–C(1)$^{\#}$–C(2)$^{\#}$–C(2).

with cyclohexane and dried in vacuum. Recrystallization from $CHCl_3$–MeOH afforded yellow crystals.[21] Yield: 80% (1.10 g). Anal. Calc. for $C_{52}H_{40}Cl_4P_4Pd_2{\cdot}2CHCl_3$: C 46.92; H 3.06. Found: C 46.57; H 3.01%. MALDI-TOF-MS (m/z): 1144.6663 (M^+ + 5), 1109.6650 (M^+ – Cl + 5), 1073.6875 (M^+ – 2Cl + 4). FT-IR (KBr, cm^{-1}): 3054 (C–H str), 1479, 1437 (Ar ip str), 1185, 1162, 1097 (oop CH def), 1027, 998 (P–Ph str), 840, 744 (oop def), 689 (ring oop def), 533, 512, 490, 475 (oop ring def). Raman (He–Ne, cm^{-1}): 2148, 2132 (C≡C), 1584, 1095, 1028, 1000, 697, 618, 570, 325, 301 (Pd–Cl), 190, 158. UV-vis (CH_3CN, λ/nm ($10^{-4}\varepsilon_{max}/M^{-1}\ cm^{-1}$)): 266 (6.65), 326 (2.38).

$(PtCl_2)_2(\mu\text{-dppa})_2$ (2). To 24 mL of an ethanol suspension of K_2PtCl_4 (2.0 mmol, 0.84 g) was added a minimum amount of degassed solvent water until the suspension became clear. A benzene solution (10 mL) of dppa (2.0 mmol, 0.79 g) was dropped into this solution, and stirred for 6 h. The white product was filtered off, and washed with distilled water and methanol consecutively. Recrystallization from $CHCl_3$–MeOH afforded yellow crystals.[34] Yield: 93% (1.23 g). Anal. Calc. for $C_{52}H_{40}Cl_4P_4Pt_2$: C 47.29; H 3.05. Found: C 47.30; H 3.05%. MALDI-TOF-MS (m/z): 1284.7332 (M^+ – Cl + 2). FT-IR (KBr, cm^{-1}): 3054 (C–H str), 1480, 1437 (Ar ip str), 1185, 1161, 1099 (oop CH def), 1027, 998 (P–Ph str), 838, 745 (oop def), 689 (ring oop def), 545, 515, 497, 445 (oop ring def). Raman (He–Ne, cm^{-1}): 2144 (C≡C), 1584, 1323, 1096, 1025, 997, 699, 614, 578, 325, 299 (Pt–Cl), 179. UV-vis (CH_3CN, λ/nm ($10^{-4}\varepsilon_{max}/M^{-1}\ cm^{-1}$)): 274 (1.98), 328 (0.26).

$[M(1,2\text{-dithiolate})]_2(\mu\text{-dppa})_2$ where M = Pd (3) and Pt (4). Each of the 1,2-benzenedithiol compounds (0.20 mmol, 29 mg for H_2**a**; 31 mg for H_2**b**; 42 mg for H_2**c**) dissolved in a minimum amount of chloroform was dropped into a chloroform solution (5 mL) of complex **1** (0.10 mmol, 110 mg) or **2** (0.10 mmol, 134 mg) with stirring for 2 h under an argon atmosphere. The orange or brown solution was dried under reduced pressure. The solid products, obtained in quantitative yield, were recrystallized from $CHCl_3$–MeOH or CH_2Cl_2–MeOH, and subjected to elemental analyses and X-ray structure analyses. The same process was followed when $[M(OTf)_2]_2(\mu\text{-dppa})_2$ (0.1 mmol) in nitromethane (5 mL) was used instead of $(MCl_2)_2(\mu\text{-dppa})_2$ in chloroform resulting in spectroscopically identical products.

3a. Yield >95%. MALDI-TOF-MS (m/z): 1283.8241 (M^+ + 4). Anal. Calc. for $C_{64}H_{48}P_4Pd_2S_4{\cdot}0.25CHCl_3$: C 58.82; H 3.71; S 9.78. Found: C 59.02; H 3.68; S 9.98%. FT-IR (KBr, cm^{-1}): 3050 (C–H str), 1550, 1479, 1437 (Ar ip str), 1098 (ip CH def), 1024, 998 (P–Ph str), 840, 740 (oop CH def), 690, 526, 510, 490, 433 (oop ring def). Raman (He–Ne, cm^{-1}): 2134 (C≡C), 1584, 1103, 1027, 998, 697, 665, 618, 561, 353 (Pd–S). UV-vis (CH_3CN, λ/nm ($10^{-4}\varepsilon_{max}/M^{-1}\ cm^{-1}$)): 260 (7.02), 304 (5.35).

3b. Yield >95%. MALDI-TOF-MS (m/z): 1310.7959 (M^+ + 3). Anal. Calc. for $C_{66}H_{52}P_4Pd_2S_4{\cdot}CHCl_3$: C 56.29; H 3.74; S 8.97. Found: C 56.07; H 3.64; S 8.94%. FT-IR (KBr, cm^{-1}): 3052 (C–H str), 2915 (–CH_3), 1542, 1480, 1458, 1436 (Ar ip str), 1097 (ip CH def), 1026, 998 (P–Ph str), 836, 743 (oop CH def), 690, 526, 511, 491 (oop ring def). Raman (He–Ne, cm^{-1}): 2146, 2131 (C≡C), 1586, 1109, 1028, 998, 556, 348 (Pd–S). UV-vis (CH_3CN, λ/nm ($10^{-4}\varepsilon_{max}/M^{-1}\ cm^{-1}$)): 268 (2.63), 320 (0.83).

3c. Yield >95%. MALDI-TOF-MS (m/z): 1421.7075 (M^+ + 6). Anal. Calc. for $C_{64}H_{44}Cl_4P_4Pd_2S_4$: C 54.14; H 3.12; S 9.03. Found: C 53.28; H 2.94; S 9.43%. FT-IR (KBr, cm^{-1}): 3053 (C–H str), 1526, 1480, 1436 (Ar ip str), 1396, 1345, 1272, 1158, 1096 (oop CH def), 1066 (C–Cl str), 1027, 998 (P–Ph str), 838, 821, 743 (oop

CH def), 690, 526, 510, 489 (oop def). Raman (He–Ne, cm^{-1}): 2130 (C≡C), 1583, 1000, 560, 362 (Pd–S). UV-vis (CH_3CN, λ/nm ($10^{-4}\varepsilon_{max}/M^{-1}$ cm^{-1})): 266 (10.7), 308 (7.37).

4a. Yield >95%. MALDI-TOF-MS (*m*/*z*): 1461.0226 (M^+ + 3). Anal. Calc. for $C_{64}H_{48}P_4Pt_2S_4{\cdot}CHCl_3$: C 49.45; H 3.13; S 8.12. Found: C 48.86; H 3.18; S 8.14%. FT-IR (KBr, cm^{-1}): 3048 (C–H str), 1550, 1480, 1437 (Ar ip str), 1099 (ip CH def), 1025, 998 (P–Ph str), 838, 741 (oop CH def), 689, 538, 513, 436 (oop ring def). Raman (He–Ne, cm^{-1}): 2149, 2133 (C≡C), 1583, 1323, 1286, 1102, 1024, 996, 570, 366 (Pt–S), 211 (Pt–P), 172. UV-vis (CH_3CN, λ/nm ($10^{-4}\varepsilon_{max}/M^{-1}$ cm^{-1})): 262 (1.91), 320 (0.30), 356 (0.26).

4b. Yield >95%. MALDI-TOF-MS (*m*/*z*): 1489.0203 (M^+ + 3). Anal. Calc. for $C_{66}H_{52}P_4Pt_2S_4{\cdot}CHCl_3$: C 50.08; H 3.32; S 7.98. Found: C 50.78; H 3.50; S 8.18%. FT-IR (KBr, cm^{-1}): 3053 (C–H str), 2918, 2859 (–CH_3), 1459, 1436 (Ar ip str), 1098 (ip CH def), 1029, 998 (P–Ph str), 837, 744 (oop CH def), 690, 538, 514, 496, 434 (oop ring def). Raman (He–Ne, cm^{-1}): 2152, 2133 (C≡C), 1582, 1323, 1283, 1205, 1109, 1024, 996, 864, 570, 365 (Pt–S), 258 (Pt–P), 167. UV-vis (CH_3CN, λ/nm ($10^{-4}\varepsilon_{max}/M^{-1}$ cm^{-1})): 266 (1.07), 326 (0.25), 358 (0.04).

4c. Yield >95%. MALDI-TOF-MS (*m*/*z*): 1598.0262 (M^+ + 4). Anal. Calc. for $C_{64}H_{44}Cl_4P_4Pt_2S_4$: C 48.13; H 2.78; S 8.03. Found: C 48.05; H 2.85; S 8.07%. FT-IR (KBr, cm^{-1}): 3055 (C–H str), 1479, 1436 (Ar ip str), 1397, 1343, 1276, 1160, 1098 (oop CH def), 1070 (C–Cl str), 1029, 999 (P–Ph str), 839, 823, 743 (oop CH def), 690, 538, 514, 494 (oop ring def). Raman (He–Ne, cm^{-1}): 2137 (C≡C), 1587, 1342, 1276, 1142, 1109, 1029, 1001, 572, 384 (Pt–S), 259 (Pt–P), 152. UV-vis (CH_3CN, λ/nm ($10^{-4}\varepsilon_{max}/M^{-1}$ cm^{-1})): 266 (2.22), 322 (0.25), 348 (0.24).

$[M(OTf)_2]_2(\mu\text{-dppa})_2$ where M = Pd (5) and Pt (6). An acetonitrile solution of Ag(OTf) (4 mmol, 1.03 g) was added to a methylene chloride solution (40 mL) of $(MCl_2)_2(\mu\text{-dppa})_2$ (1 mmol, 1.14 g for M = Pd and 1.32 g for M = Pt) with stirring for 4 h under an argon atmosphere. The white precipitate (AgCl) was separated by filtration through a fine glass filter and washed with a minimum amount of acetonitrile, and the filtrate was centrifuged at 15 000 rpm for 2 h. The filtrate was dried under reduced pressure and recrystallized. The crystalline products were obtained in quantitative yield and used directly in the synthesis of complexes **3** or **4**.

5. Yield >95%. FT-IR (KBr, cm^{-1}): 3057 (C–H str), 1481, 1437 (Ar ip str), 1261, 1173, 1099 (ip CH def), 1033 (SO_3CF_3), 998 (P–Ph str), 840, 744 (oop CH def), 689, 512, 493, 474 (oop ring def).

6. Yield >95%. FT-IR (KBr, cm^{-1}): 3056 (C–H str), 1481, 1438 (Ar ip str), 1262, 1173, 1099 (ip CH def), 1034 (SO_3CF_3), 998 (P–Ph str), 840, 745 (oop CH def), 689, 515, 497, 442 (oop ring def).

Results and discussion

Synthesis and vibrational spectroscopic analysis

As shown in Scheme 2, complex **2** was prepared by mixing equal amounts of K_2PtCl_4 in H_2O and dppa in benzene using a minimum amount of ethanol as a mediator:[15] Even though H_2O and benzene do not normally mix with each other, the ethanol solvent facilitates the mixing of these two immiscible solvents, resulting in the formation of a mixed-solvent system (water–ethanol–benzene). It can be supposed that the two reactants are completely dissolved in the mixed-solvent system and can readily react with each other, and actually a high yield of the product of about 93% was obtained. The reaction was almost completed after 1 h, and the chemical compositions of the products were confirmed by elemental analysis and MALDI-TOF-MS measurements. The synthesis of complex **1** was, however, achieved following the reported method[21] and afforded a fairly high yield (80%).

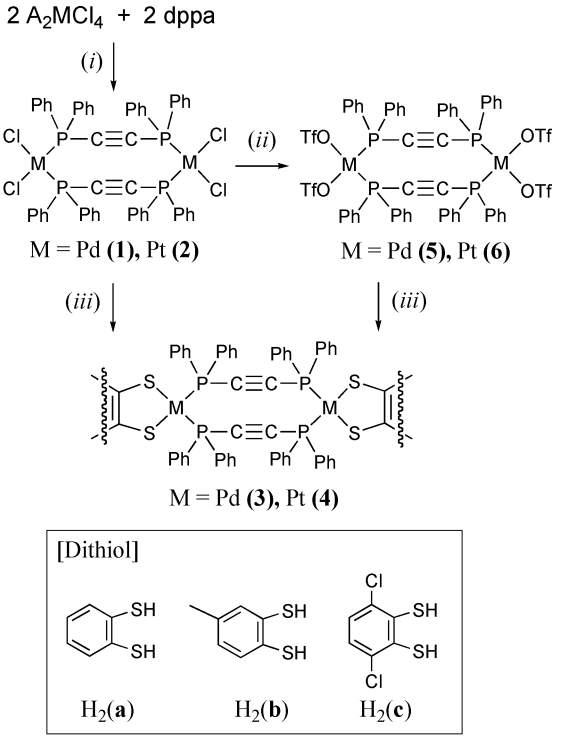

Reaction conditions: (*i*) EtOH (M = Pd, A = Na) *or* H_2O/EtOH/Bz (M = Pt, A = K), (*ii*) 4Ag(OTf)/CH_3CN, (*iii*) [Dithiol], $CHCl_3$.

Scheme 2

Complexes **3** and **4** were synthesized by reacting 1,2-benzenedithiolates (bdts) with $[M(OTf)_2]_2(\mu\text{-dppa})_2$, as well as $(MCl_2)_2(\mu\text{-dppa})_2$, in a high yield as shown in Scheme 2. The products prepared through the two different pathways were spectroscopically identical. One merit for the use of $[M(OTf)_2]_2(\mu\text{-dppa})_2$ is that the pure products can be obtained even before the chromatographic purification step. Complexes **3** and **4** dissolved in an appropriate solvent were treated either with UV-radiation or elevated temperatures to induce intramolecular cyclization in a similar manner to that observed with binuclear Pt-(*trans*-dppen)[17] and Pt-dppby[18] complexes. Our complexes, however, did not show any evidence of cyclization under these conditions, possibly due to the lack of the flexibility of the dppa ligand.

The Pd(II) and Pt(II) complexes synthesized in this research give very rich IR and Raman spectra exhibiting P–C, C=C, C≡C and C–H vibrations from the ligands and M–Cl, M–P and M–S vibrations from the coordination sphere. All of the complexes show strong C=C vibrational bands of aromatic rings at *ca.* 1480–1430 cm^{-1} and C–H stretching bands at *ca.* 830–680 cm^{-1}. The P–Ph vibrations are observed at an almost fixed position (997–1000 cm^{-1}) in the IR/Raman spectra, regardless

of whether they have MP_2Cl_2 or MP_2S_2 cores, which indicates that the P–Ph vibrations are completely free from the influence of the central metals and the other coordination ligands such as Cl and S (from 1,2-dithiolate). The IR-inactive but Raman-active vibrational mode of the symmetric C≡C bond[40] appears at 2100 cm^{-1} in the spectra of free dppa, but those of complexes **1–4** are detected as strong peaks in the range of 2130–2152 cm^{-1}. The wavenumber shifts of about 30–52 cm^{-1} indicate the coordination of M(II) to the phosphorus atom, not the C≡C bond, because the P→M coordination can cause the weakening of the pπ–dπ overlap on the ≡C–P bond and the consequent increase of the vibrational frequency of the C≡C bond. When the C≡C bond instead of a phosphine ligand is coordinated to a metal ion, the local symmetry is generally lowered and ν(C≡C) usually shifts to a lower frequency by 200–400 cm^{-1}. For the structures having C_{2v} symmetry, such as *cis*-MP_2Cl_2 core, group theory predicts that the Raman active ν(M–X) vibrational modes (A_1 + B_1) will be found at around 300 cm^{-1}.[41] These halogen-sensitive absorptions were observed in the Raman spectra at 325 and 301 cm^{-1} for the ν(Pd–Cl) vibrations of complex **1** and at 325 and 299 cm^{-1} for the ν(Pt–Cl) vibrations of complex **2**. The ν(M–S) vibrations of the *cis*-MP_2S_2 core with the 1,2-dithiolate ligand are generally observed in the range of 300–400 cm^{-1}.[15,16,34,35] As regards the Raman spectra of complexes **3** and **4**, the ν(Pd–S) vibrations were observed at 348 cm^{-1} (**3b**), 353 cm^{-1} (**3a**) and 362 cm^{-1} (**3c**), while the ν(Pt–S) vibrations were observed at 365 cm^{-1} (**4b**), 366 cm^{-1} (**4a**) and 384 cm^{-1} (**4c**). It is clearly shown from these data that the ν(M–S) vibrational frequencies are very sensitively proportional to the electron-donating ability of the 1,2-dithiolate ligands with the order of tdt (**b**) ≈ bdt (**a**) > Cl_2bdt (**c**).

^{1}H, ^{31}P and ^{195}Pt NMR spectroscopic analyses

Complexes **1–4** were characterized by $^{31}P\{^1H\}$ and/or $^{195}Pt\{^{31}P\}$ NMR spectroscopies and their parameters are collected in Table 1 and 2. The ^{31}P NMR spectra of complex **3** give a singlet at 1.676–1.943 ppm with an approximately 3 ppm up-field shift relative to that of complex **1**. On the other hand, complex **4** shows the typical 1 : 4 : 1 signals with a down-field shift of about 9 ppm in its ^{31}P NMR spectra and an up-field shift of about 269–298 ppm in its ^{195}Pt NMR spectra relative to complex **2**, surely due to the electron-donating properties of the 1,2-dithiolate ligands. Furthermore, the 1,2-benzenedithiolate ligand with an electron-withdrawing moiety in complex **4c** would be expected to exhibit the lowest electron donating ability among the three dithiolates. It is evidenced from the observations that the value of δ_{Pt} for complex **4c** (–4700 ppm) is significantly downfield shifted. However, the methyl moiety on the ligand **b** does not play a significant role in the variation of the δ_{Pt} value between complexes **4a** and **4b**. These results coincide well with the vibrational spectroscopic results, in that the ν(Pt–S) vibrations for **4a** and **4b** are very close to each other (366 and 365 cm^{-1}, respectively), whereas that of **4c** was observed in a higher frequency region (384 cm^{-1}).

The magnitude of the Pt–P coupling (J_{Pt-P}) for complex **4** fell in the range of 2800–2814 Hz, suggesting the *cis* coordination of the phosphine ligands, as observed in *cis*-$(Ph_3P)_2$Pt(dithiolates).[8,42] The variation of the NMR parameters is closely related to the electron-donating ability of the dithiolate ligands. The J_{Pt-P} values are sensitive to the electron-donating properties of the dithiolate ligand,[8] and increased in the following order: **4c** < **4b** ≈ **4a**. This can also be explained by the inductive effect of the substituted ligands. The amount of P→Pt donation is inversely proportional to the electron-withdrawing ability of the 1,2-dithiolate ligands resulting in a higher field resonance and a weaker Pt–P coupling.

X-Ray crystal structure determinations

The X-ray structure determination for single crystals of **3** and **4** was performed at room temperature. The crystal data and the information used for the structure refinements are listed in Table 3, and the selected bond lengths (Å) and angles (°) are listed in Table 4. Fig. 1–6 show the X-ray crystal structures of complexes **3** and **4**. The observed Pd–P (2.278(1)–2.312(1) Å), Pd–S (2.277(1)–2.293(1) Å), Pt–P (2.258(2)–2.293(2) Å) and Pt–S (2.293(2)–2.314(2) Å) bond lengths of the complexes are slightly shorter than the sum of their covalent radii (2.34, 2.30, 2.36 and 2.32 Å, respectively).[43] The Pt–P and Pt–S bond distances are similar to those of $[Pt(MET)]_2(\mu\text{-dppa})_2$ (2.264(3) and 2.288(3) Å, respectively) where MET is (*Z*)-1,4-dimethoxy-1,4-dioxobut-2-ene-2,3-bis(thiolate).[35] On the other hand, the Pt–S bond length of $[Pt(PFBT)_2]_2(\mu\text{-dppa})_2$ (2.349(3) Å; PFBT = pentafluorobenzenethiolate)[24] is longer than those of **4a** (2.305(2) Å), **4b** (2.303(2) Å) and **4c** (2.301(2) Å), possibly due to the presence of the mono-dentate PFBT ligand and the effect of the five electronegative fluorides on the PFBT ligand, while the Pt–P bond lengths (2.272(3) Å) are similar to those of **4** (2.258(2)–

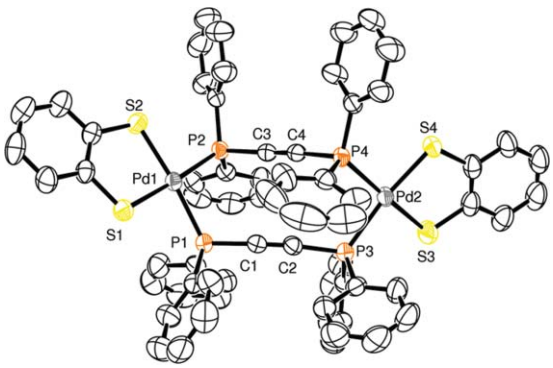

Fig. 1 Molecular structure of $[Pd(bdt)]_2(\mu\text{-}Ph_2PC{\equiv}CPPh_2)_2$ (**3a**) with thermal ellipsoids drawn at the 50% probability level. Solvent molecules and hydrogen atoms are omitted for clarity.

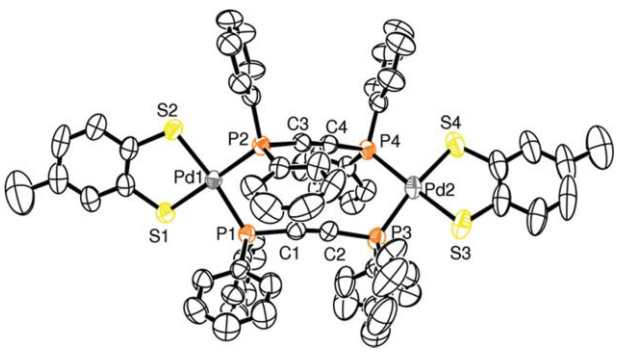

Fig. 2 Molecular structure of $[Pd(tdt)]_2(\mu\text{-}Ph_2PC{\equiv}CPPh_2)_2$ (**3b**) with thermal ellipsoids drawn at the 50% probability level. Hydrogen atoms are omitted for clarity.

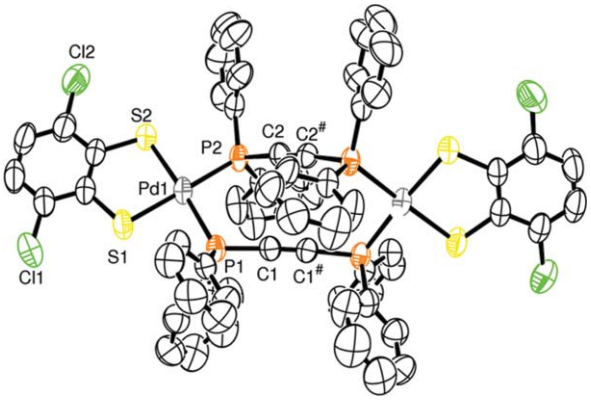

Fig. 3 Molecular structure of $[Pd(Cl_2bdt)]_2(\mu\text{-}Ph_2PC{\equiv}CPPh_2)_2$ (**3c**) with thermal ellipsoids drawn at the 50% probability level. Hydrogen atoms are omitted for clarity (symmetry transformations used to generate equivalent atoms: # $-x + 1, y, -z + 3/2$).

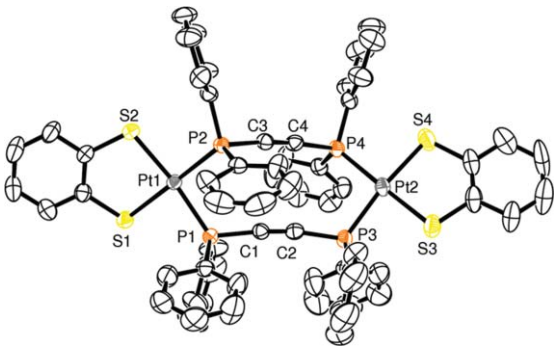

Fig. 4 Molecular structure of $[Pt(bdt)]_2(\mu\text{-}Ph_2PC{\equiv}CPPh_2)_2$ (**4a**) with thermal ellipsoids drawn at the 50% probability level. Solvent molecules and hydrogen atoms are omitted for clarity.

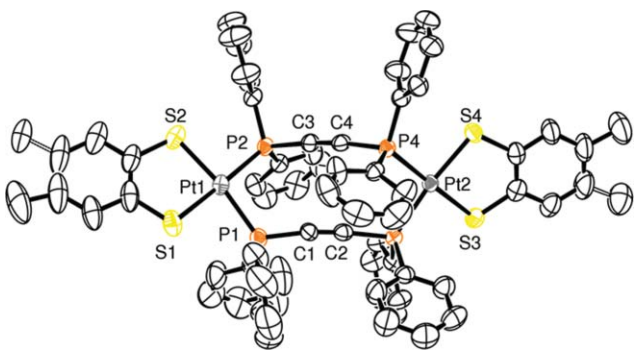

Fig. 5 Molecular structure of $[Pt(tdt)]_2(\mu\text{-}Ph_2PC{\equiv}CPPh_2)_2$ (**4b**) with thermal ellipsoids drawn at the 50% probability level. Solvent molecules and hydrogen atoms are omitted for clarity. The disordered methyl groups are shown in the figure.

2.293(2) Å). When the electronegative chloride ions are directly ligated to the Pt(II) ion as in $[PtCl_2]_2(\mu\text{-dppa})_2$, however, the average Pt–P bond distance (2.239(2) Å)[34] becomes much shorter than those of **4** because of the inductive effect of the electronegative ions. The averaged bond lengths of Pt–P (2.270(2) Å for **4a**, 2.269(2) Å for **4b**, and 2.281(2) Å for **4c**) are inversely correlated with the value of the Pt–P coupling constant (J_{Pt-P}: 2814, 2813 and 2800 Hz, respectively; Table 2). This can be explained by the simple rationale that the degree of spin-coupling of the Pt and P nuclei is decreased

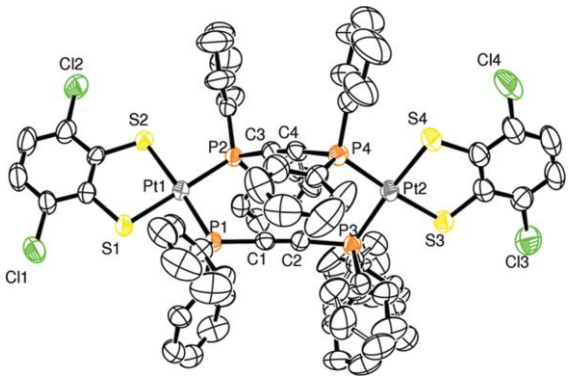

Fig. 6 Molecular structure of $[Pt(Cl_2bdt)]_2(\mu\text{-}Ph_2PC{\equiv}CPPh_2)_2$ (**4c**) with thermal ellipsoids drawn at the 50% probability level. Solvent molecules and hydrogen atoms are omitted for clarity. The disordered phenyl groups are shown in the figure.

as the distance between them (that is, the Pt–P bond length) is increased.

The P–M–S *trans* angles are within the range of 170.22(7)–177.86(7)°, which reveals that the P_2MS_2 core slightly deviates from the complete square-planar geometry, and the C≡C bond distances (1.177(9)–1.206(6) Å) are also slightly shorter than that in acetylene (1.21 Å). The two acetylenic moieties in one molecule are staggered relative to each other with a torsion angle of C(1)–C(2)–C(4)–C(3), as shown in Table 4, where the torsion angles of complexes **3c** and **4c** containing ligand **c** are larger (about 42°) than those of the other complexes (22–31°). The P–C≡C bond angles deviate from linearity, with their average values of 172.9°–173.6° (**3a**, **3b**, **4a** and **4b**), 175.9° (**3c**) and 175.4° (**4c**) being larger than those of the bis(monothiolate) derivatives such as $[Pt(PFBT)_2]_2(\mu\text{-dppa})_2$ (171.3(7)°).[24] These observations indicate that complexes **3** and **4**, especially complexes **3c** and **4c**, are totally distorted, which is common in the complexes of $(ML_n)_2(\mu\text{-dppa})_2$ where ML_n is Pt(MET),[35] $Ru(acac)_2$,[33] $Pt(C_6F_5)_2$,[32] $Pt(PFBT)_2$,[24] and $Mo(CO)_4$.[31] Furthermore, they are distorted in right- and left-handed modes and their crystals are racemic, as shown in Fig. S4–S9 (see ESI†).

Electrochemical study

The electrochemical properties of complexes **1**, **2**, **3** and **4** were investigated by cyclic voltammetry (CV). The potentials were swept forward from −1.0 to +2.0 V and then back again. The cyclic voltammograms of complexes **2**, **3** and **4** are shown in ESI (Fig. S1–S3),† and their electrochemical parameters are listed and compared in Table 5. Complex **1** exhibits one irreversible oxidation peak at E_{pa} = 1.102 V, but it seems to be unstable in solution, because of the lack of reproducibility of the results. One quasi-reversible cycle with E_{pa} = 1.334 V and E_{pc} = 1.028 V, however, was observed for complex **2**, in which the anodic peak can be attributed to the Pt-centered oxidation. On the contrary, complexes **3** and **4** show two irreversible anodic peaks in the range of 0.9–1.5 V, as summarized in Table 5. It is worthwhile comparing them with the previously reported $[Pt(1,2\text{-ethylenedithiolate})]_2(\mu\text{-dppa})_2$ complexes.[34] These complexes showed two redox peaks in which one reversible cycle that appears at around $E_{1/2}$ = 0.745–1.010 V (*vs.* Ag/Ag^+) is attributable to the redox process of the 1,2-ethylenedithiolate ligand and the other one found at

Table 5 Cyclic voltammetry parameters for complexes **1**, **2**, **3** and **4**[a]

Complex	E_{pa}^{1}/V[b]	E_{pa}^{2}/V[b]
1	—	1.102
2	1.028[c]	1.334
3a	0.983	1.091
3b	0.972	1.030
3c	1.142	1.371
4a	1.073	1.247
4b	1.046	1.204
4c	1.230	1.480

[a] Samples are dissolved in CH_2Cl_2 (1.0 mM, 10 mL) containing 0.1 M n-Bu_4NBF_4 electrolyte and measured with a scan rate of 50 mV s^{-1}. Ag/Ag^+ reference electrode, a Pt-button working electrode ($r = 1$ mm) and a Pt-wire counter electrode are used. [b] Fc/Fc^+: $E_{1/2} = +0.687$ V. [c] E_{pc}^{1}/V.

around $E_{pa} = 1.420$–1.506 V (*vs.* Ag/Ag^+) is ascribed to the Pt-centered oxidation. In the present system (complexes **3** and **4**) also, the first irreversible anodic peak (E_{pa}^{1}) corresponds to the oxidation process of the 1,2-benzenedithiolate ligands and the second one (E_{pa}^{2}) corresponds to the Pt-center. Moreover, the anodic potentials of **3a**, **3b**, **4a** and **4b** are 0.16–0.34 V lower than those of the corresponding complexes **3c** and **4c**. This clearly indicates the ease of oxidation of the 1,2-benzendithiolate ligands in the order of **b** ≈ **a** ≫ **c**, based on the electrochemical results.

Absorption and emission spectra

The absorption spectra of the synthesized complexes showed a band centered at ~265 nm and additional small bands between 304 and 360 nm in solution, as shown in the Experimental section. Overall, the observed spectra of the platinum complexes are similar to those of the dithiol ligands except a ~40 nm red shift upon complex formation. The lowest energy band at 360 nm was observed with **4a** and no additional absorption band was observed in the wavelength region longer than ~400 nm for all complexes (see ESI†).

Among the six metal-dithiolate complexes prepared in this study, only complex **4c** was luminescent at room temperature in the solid state whereas no emission was observed in solution. This emission band was broad with a maximum at 615 nm. However, the excitation spectrum was structured so as to exhibit vibrational progressions and centered at 430 nm (Fig. 7). The Stokes shift (~7000 cm^{-1}) was relatively large. The metal-metal-to-ligand charge transfer transition (MMLCT) can be ruled out for **4c** since there is no direct interaction between the platinum metals as evidenced by the large metal-to-metal distance (7.265 and 8.007 Å for the shortest Pd···Pd and Pt···Pt distances, respectively) determined from its X-ray crystal structure. In addition, it is highly unlikely that this emission originates from the transition between the ligands. Neither the analogous palladium complexes nor the ligands by themselves showed luminescence at 615 nm. The X-ray crystal structure also revealed that the formation of an excimer or exciplex between the ligands is unfeasible.

Based on the fact that only the complex containing the ligand **c** and Pt(II) ion exhibited luminescence, the transition required to generate the emissive state can be assigned as the d–$\pi^*_{dithiolate}$ metal-to-ligand charge transfer (MLCT). The transition probability of the MLCT band is known to increase as the ligand becomes more reducible or electronegative. The ligand **c** has a larger

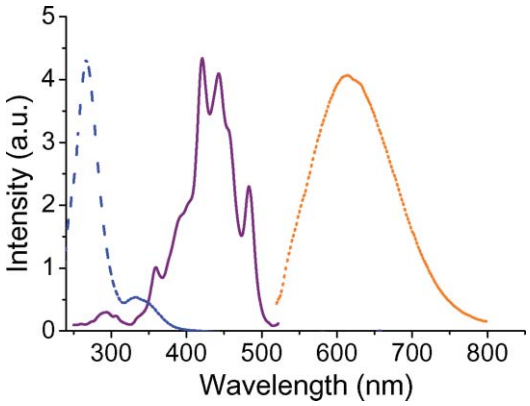

Fig. 7 Absorption (dashed blue), excitation (solid purple) and emission (dotted orange) spectra of complex **4c** in the solid state at 298 K (time-resolved detection: 5 ms flash period, 10 μs decay; excitation: λ_{ob} = 610 nm, 16/16 band pass, 700 V; emission: λ_{ex} = 440 nm, 16/16 band pass, 680 V).

electronegativity than both **a** and **b** as evidenced by the fact that the ^{195}Pt NMR chemical shift of **4c** is the most downfield shifted. The highest oxidation potential of **4c**, as measured by cyclic voltammetry, supports this assignment as well.

In addition, there are many indications that this emission involves a spin-forbidden transition. The 430 nm excitation band is not observed in the absorption spectrum of **4c** in solution, implying that its extinction coefficient is small. Also, we found that the luminescence lifetime is moderately long (≥5 μs), which strongly signifies that it has spin-forbidden characteristics. Therefore, we can assign the emissive state of **4c** as $^3\{d–\pi^*_{dithiolate}\}$. Undoubtedly, the more effective spin–orbit coupling of ligand **c** in complex **4c** containing heavy chlorine atoms, as compared to that in the ligands **a** and **b**, contributed to the feasibility of this spin-forbidden transition. The larger spin–orbit coupling in platinum than that in palladium may also contribute to the transition probability. It should be noted that our findings and the assignment for the emission band are similar to those previously reported for Pt(II) complexes containing dithiolate ligands.[10,44] In the previous studies, the luminescence of the synthesized complexes was observed only in the solid state and the luminescent platinum complexes exhibited a long luminescence lifetime and a small extinction coefficient, confirming that the emissive state was $^3\{d–\pi^*_{dithiolate}\}$.

Conclusions

As part of a serial investigation of Pd(II) and Pt(II) co-ordination complexes, the heteroleptic binuclear complexes, $[M(bdts)]_2(\mu\text{-dppa})_2$ (M = Pd (**3**) and Pt (**4**); dppa = 1,2-bis(diphenylphosphino)acetylene = $Ph_2PC{\equiv}CPPh_2$; bdts = 1,2-benzenedithiolate (bdt; **a**), 3,4-toluenedithiolate (tdt; **b**) and 1,4-dichloro-2,3-benzenedithiolate (Cl_2bdt; **c**)) were prepared using $(MCl_2)_2(\mu\text{-dppa})_2$ (M = Pd (**1**) and Pt (**2**)). The X-ray crystal structure analyses of **3** and **4** show that they are twisted in two ways and, thus, their single crystals are racemic mixtures. The more electronegative ligand **c** (and its complexes **3c** and **4c**), as compared to ligands **a** and **b**, leads to higher ν(M–S) vibrational frequencies in the Raman spectra, a smaller spin–spin coupling constant ($J_{Pt\text{-}P}$) in the $^{195}Pt\{^{31}P\}$ NMR spectra, higher anodic potentials (E_{pa}) in

the cyclic voltammograms and larger torsion angles than those of complexes **3a**, **3b**, **4a** and **4b**. Moreover, only complex **4c** exhibits luminescence ($\lambda_{ob} = 610$ nm and $\lambda_{ex} = 440$ nm) in the solid state at 298 K, assigned as the d–$\pi^*_{dithiolate}$ metal-to-ligand charge transfer (MLCT).

Acknowledgements

This work was supported by Korea Research Foundation Grant (KRF-2003-070-C00029).

Notes and references

1 V. K. Jain and L. Jain, *Coord. Chem. Rev.*, 2005, **249**, 3075–3197.
2 E. I. Stiefel, Dithiolene Chemistry: Syntheses, Properties and Applications, *Prog. Inorg. Chem.*, 2004, **52**, 315–368.
3 K. M. Wong, C. Hui, K. Yu and V. W. Yam, *Coord. Chem. Rev.*, 2002, **229**, 123–132.
4 M. Hissler, J. E. McGarrah, W. B. Connick, D. K. Geiger, S. D. Cummings and R. Eisenberg, *Coord. Chem. Rev.*, 2000, **208**, 115–137.
5 W. Paw, S. D. Cummings, M. A. Mansour, W. B. Connick, D. K. Geiger and R. Eisenberg, *Coord. Chem. Rev.*, 1998, **171**, 125–150.
6 A. Vogler and H. Kunkely, *Coord. Chem. Rev.*, 2002, **230**, 243–251.
7 C. J. Smith, V. S. Reddy, S. R. Karra, K. V. Katti and L. J. Barbour, *Inorg. Chem.*, 1997, **36**, 1786–1791.
8 C. E. Keefer, R. D. Bereman, S. T. Purrington, B. W. Knight and P. D. Boyle, *Inorg. Chem.*, 1999, **38**, 2294–2302; C. E. Keefer, S. T. Purrington, R. D. Bereman, B. W. Knight, D. R. Bedgood and P. D. Boyle, *Inorg. Chim. Acta*, 1998, **282**, 200–208.
9 J. M. Bevilacqua and R. Eisenberg, *Inorg. Chem.*, 1994, **33**, 2913–2923.
10 J. M. Bevilacqua, J. A. Zuleta and R. Eisenberg, *Inorg. Chem.*, 1994, **33**, 258–266.
11 S. P. Kaiwar, A. Vodacek, N. V. Blough and R. S. Pilato, *J. Am. Chem. Soc.*, 1997, **119**, 3311–3316.
12 K. A. Van Houten, D. C. Heath, C. A. Barringer, A. L. Rheingold and R. S. Pilato, *Inorg. Chem.*, 1998, **37**, 4647–4653; K. A. Van Houten, N. V. Blough and R. S. Pilato, *Inorg. Chim. Acta*, 2003, **353**, 231–237.
13 N. Lardies, E. Cerrada and M. Laguna, *Polyhedron*, 2006, **25**, 2785–2790.
14 L. L. Maisela, A. M. Crouch, J. Darkwa and I. A. Guzei, *Polyhedron*, 2001, **20**, 3189–3200.
15 D. Y. Noh, E. M. Seo, H. J. Lee, H. Y. Jang, M. G. Choi, H. Y. Kim and J. Hong, *Polyhedron*, 2001, **20**, 1939–1945.
16 K. S. Shin, Y. K. Han and D. Y. Noh, *Bull. Korean Chem. Soc.*, 2003, **24**, 235–238.
17 W. Oberhauser, T. Stampfl, C. Bachmann, R. Haid, C. Langes, H. Kopacka, K.-H. Ongania and P. Brüggeller, *Polyhedron*, 2000, **19**, 913–923; W. Oberhauser, C. Bachmann, T. Stampfl, R. Haid, C. Langes, H. Kopacka, A. Rieder and P. Brüggeller, *Inorg. Chim. Acta*, 1999, **290**, 167–179.
18 M. P. Martin-Redondo, L. Scoles, B. T. Sterenberg, K. A. Udachin and A. J. Carty, *J. Am. Chem. Soc.*, 2005, **127**, 5038–5039.
19 D. Liu, Q. Feng, X. L. Feng and J. W. Cai, *Inorg. Chem. Commun.*, 2003, **6**, 361–364.
20 C. H. Chou, W. Y. Yeh, G. H. Lee and S. M. Peng, *Inorg. Chim. Acta*, 2006, **359**, 4139–4143.
21 A. J. Carty and A. Efraty, *Inorg. Nucl. Chem. Lett.*, 1968, **4**, 427–431.
22 A. J. Carty and A. Efraty, *Chem. Commun. (London)*, 1968, 1559–1561.
23 W. Oberhauser, C. Bachmann, T. Stampfl and P. Brüggeller, *Inorg. Chim. Acta*, 1997, **256**, 223–234.
24 A. Singhal, V. K. Jain and R. J. Butcher, *J. Coord. Chem.*, 1999, **46**, 355–363.
25 A. J. Carty and A. Efraty, *Inorg. Chem.*, 1969, **8**, 543–550.
26 H. C. Clark, G. Ferguson, P. N. Kapoor and M. Parvez, *Inorg. Chem.*, 1985, **24**, 3924–3928.
27 J.-L. Chen, L.-Y. Zhang, Z.-N. Chen, L.-B. Gao, M. Abe and Y. Sasaki, *Inorg. Chem.*, 2004, **43**, 1481–1490; E. Louattani and J. Suades, *J. Organomet. Chem.*, 2000, **604**, 234–240; B. F. G. Johnson, J. Lewis, A. D. Massey, P. R. Raithby and W. T. Wong, *J. Organomet. Chem.*, 1990, **397**, C28–C30; O. Orama, *J. Organomet. Chem.*, 1986, **314**, 273–279; G. R. Eaton and R. H. Holm, *Inorg. Chem.*, 1971, **10**, 805–811; A. J. Carty, A. Efraty, T. W. Ng and T. Birchall, *Inorg. Chem.*, 1970, **9**, 1263–1268; A. J. Carty, A. Efraty and T. W. Ng, *Can. J. Chem.*, 1969, **47**, 1429–1431; W. A. Anderson, A. J. Carty and A. Efraty, *Can. J. Chem.*, 1969, **47**, 3361–3366.
28 A. J. Carty and A. Efraty, *Can. J. Chem.*, 1969, **47**, 2573–2578.
29 K. S. Wheelock, J. H. Nelson and H. B. Jonassen, *Inorg. Chim. Acta*, 1970, **4**, 399–403.
30 C. M. Bolinger and T. B. Rauchfuss, *Inorg. Chem.*, 1982, **21**, 3947–3954.
31 G. Hogarth and T. Norman, *Polyhedron*, 1996, **15**, 2859–2867.
32 L. R. Falvello, J. Fornies, J. Gomez, E. Lalinde, A. Martin, F. Martinez and M. T. Moreno, *J. Chem. Soc., Dalton Trans.*, 2001, 2132–2140.
33 M. A. Bennett, M. J. Byrnes and A. C. Willis, *Dalton Trans.*, 2007, 1677–1686.
34 K. S. Shin and D. Y. Noh, *Bull. Korean Chem. Soc.*, 2004, **25**, 130–132.
35 D. Y. Noh, K. S. Shin and K. I. Son, *Bull. Korean Chem. Soc.*, 2007, **28**, 343–346.
36 G. M. Sheldrick, *SADABS, A Program for Area Detector Absorption Corrections*, University of Göttingen, Germany, 1994.
37 G. M. Sheldrick, *SHELXTL, version 5*, Bruker AXS, Madison, WI, 1995.
38 P. van der Sluis and A. L. Spek, *Acta Crystallogr., Sect. A: Found. Crystallogr.*, 1990, **46**, 194–201.
39 A. L. Spek, *J. Appl. Crystallogr.*, 2003, **36**, 7–13.
40 R. M. Silverstrein, G. C. Bassler and T. C. Morrill, *Spectroscopic Identification of Organic Compounds*, Wiley, Singapore, 5th edn, 1991, pp. 107–108.
41 K. Nakamoto, *Infrared and Raman Spectra of Inorganic and Coordination Compounds, Part A*, John Wiley & Sons, NY, 5th edn, 1997.
42 S. O. Grim, R. L. Keiter and W. Mcfarlane, *Inorg. Chem.*, 1967, **6**, 1133–1137.
43 J. A. Dean, in *Lange's Handbook of Chemistry*, McGraw Hill, NY, 15th edn, 1999.
44 J. M. Bevilacqua, J. A. Zuleta and R. Eisenberg, *Inorg. Chem.*, 1993, **32**, 3689–3693.